Generation of vacancy-type point defects in single collision cascades during swift-ion bombardment of silicon

B. G. Svensson
Royal Institute of Technology, Solid State Electronics, P. O. Box E229, S-164 40 Kista-Stockholm, Sweden

C. Jagadish
Department of Electronic Materials Engineering, Research School of Physical Sciences and Engineering, Canberra ACT 0200, Australia

A. Hallén*
Department of Radiation Sciences, Uppsala University, P.O. Box 535, S-751 21 Uppsala, Sweden

J. Lalita
Royal Institute of Technology, Solid State Electronics, P.O. Box E229, S-164 40 Kista-Stockholm, Sweden
(Received 13 December 1996)

Silicon samples of n-type have been implanted with low doses (10^7-10^{10} cm^{-2}) of ^{11}B, ^{12}C, ^{16}O, ^{28}Si, ^{74,76}Ge, and ^{120}Sn ions using energies between 0.4 and 8.0 MeV. Because of the low doses employed, single-collision cascades prevail, and an analysis of the implanted samples by deep-level transient spectroscopy (DLTS) reveals two dominant point defects of vacancy type, the divacancy (V_2) and the vacancy-oxygen (VO) center. The generation of V_2 and VO is studied in detail as a function of ion mass, dose, dose rate, sample depth, and sample temperature. Surface-enhanced annihilation of migrating defects is found to play a significant role in depleting the concentration of V_2 and VO centers in proximity to the surface. The concentration of V_2 and VO increases linearly with ion dose, but the generation efficiency per incoming ion decreases at high dose rates after displaying a constant value below $\sim 10^8$ cm^{-2} s^{-1}. This dose rate effect exhibits a dependence on ion mass, and is qualitatively predicted by computer simulations of the defect reaction kinetics, applying a model where the interaction between individual collision cascades is primarily due to fast-diffusing Si self-interstitials. At dose rates $\leqslant 10^8$ cm^{-2} s^{-1}, the generation of V_2 centers per ion-induced vacancy in the damage peak region is identical, within $\pm 10\%$, for all the different types of ions studied. However, the V_2 centers formed by heavy ions are strongly perturbed, as shown by large deviations from a one-to-one relation between the two DLTS peaks associated with the singly and doubly negative charge state of V_2, and also by a broadening of the two peaks. In contrast to that for V_2, the generation of VO centers per ion-induced vacancy decreases with increasing ion mass, consistent with the picture that light ions are more effective in generating point defects than heavy ions. At elevated implantation temperatures, gradual relaxation of lattice strain occurs together with recrystallization of disordered zones, promoting the formation of unperturbed V_2 centers and increasing the generation efficiency of VO centers. [S0163-1829(97)09915-3]

I. INTRODUCTION

The displacement energy threshold for target atoms in crystalline semiconductors is in the range of 10–40 eV, and consequently, bombardment with any type of ions having energies in excess of ~ 100 eV gives rise to pairs of vacancies and recoiling target atoms. The creation of such Frenkel pairs is predominantly determined by the elastic collision cross section, which depends on the mass of the incoming ions, the target atom mass, and the incident ion energy, having a maximum around $\varepsilon \sim 0.3$, where ε is the reduced energy introduced by Lindhard *et al.*[1] For swift ions with energies in the MeV range, electronic stopping dominates initially, and elastic collisions prevail toward the end of the ion track. This implies a nonuniform distribution of defects peaking at large depths, where a high concentration of vacancies and target self-interstitials occurs. For example, assuming a displacement energy threshold of 13 eV,[2] Monte Carlo calculations using the transport of ions in matter code (TRIM, version -90) (Ref. 3) yield an average generation rate of more than one vacancy per Å and ion in the damage peak region for bombardment of silicon with MeV Ge ions. This suggests formation of complex defect clusters by single ions, but the probability for recombination between vacancies (V's) and self-interstitials (I's) is normally very large in semiconductors. In silicon, only a few percent of the vacancies escape annihilation with Si interstitials and are left to form point defects stable at room temperature (RT).[4,5] These conclusions are mainly based on experimental data, but are also consistent with recent results from molecular-dynamics (MD) simulations showing that very few isolated Frenkel pairs are produced by single-collision cascades.[6] According to MD simulations, isolated point defects are predominantly due to replacement collision sequences along low-index crystallographic axes, and, since these sequences are short relative to the radius for spontaneous annihilation, the probability of creating ''stable'' pairs of V's and I's is small. On the other hand, the MD simulations also suggest that large pockets of unrelaxed disordered material are produced by the collision cascades. These disordered regions are amor-

phouslike with large surface-to-volume ratios and surrounded by crystalline material which make them recrystallize much faster than a stable planar amorphous-crystal interface.

Despite the fact that considerable efforts have been made by several groups to study the evolution of damage in crystalline silicon during ion implantation, which ultimately gives rise to a crystal-to-amorphous phase transformation, no consensus has been reached. Some authors discussed a process based on accumulation of point defects,[7] while others favored a mechanism involving overlap of intracascade-generated amorphous zones.[8] However, no model accounts for all the experimental observations,[9] and large uncertainties exist for several fundamental properties, e.g., different estimates of the diffusivity of I differ by ten orders of magnitude or even more.[10] In this study, we focus on the formation of vacancy-type defects during the initial state of ion bombardment where single-collision cascades prevail, and the overlap between different ion tracks is small. In such a dilute concentration regime, defects in semiconductors are most appropriately investigated by means of optical and electrical methods,[11–17] e.g., infrared spectroscopy (IR), photoconductivity, electron paramagnetic resonance (EPR) techniques, photoluminescence (PL), and deep-level transient spectroscopy (DLTS). In particular, DLTS has recently proven to be highly suitable because of its extreme sensitivity, where specific defects with distinct signatures and concentrations of $\sim 10^{-5}-10^{-6}$ of the dopant concentration can be monitored.[17] Moreover, in DLTS, defect concentration versus depth profiles can be obtained. However, the assignment of the observed signatures (energy-level position in the band gap and capture cross sections of charge carriers) with specific defect centers is not trivial, and correlation with data from other techniques is required.

Point defects in crystalline silicon induced by MeV electron irradiation have been extensively studied by many authors for more than 30 years applying a variety of experimental methods such as EPR, IR, DLTS, PL, and electron-nuclear double resonance.[11,12,14–18] In this context it should be emphasized that, in contrast to energetic ions, MeV electrons give rise to a uniform distribution of isolated and unperturbed point defects over depths of several millimeters. Vacancy-type defects of major importance in silicon, having well-established signatures and being stable after irradiation at RT, are the centers of vacancy-oxygen (VO), divacancy (V_2), and vacancy-group V atom (the E center or VP, VAs, and VSb, depending on the type of dopant atoms used). VO is formed through the capturing of migrating vacancies by interstitial oxygen atoms (O_i), which are the main impurity atoms in Czochralski-grown (Cz) silicon. This defect, the so-called A center, was first reported more than 35 years ago;[11,14,19,20] the oxygen atom occupies a position slightly displaced from the central tetrahedral substitutional site in a $\langle 100\rangle$ direction, and bonds to two silicon atoms. In contrast to O_i, VO is electrically active, with an acceptor level located ~ 0.18 eV below the conduction-band edge (E_c);[11,14] ($-/0$; of the charge state $-$ if the level is occupied by an electron, and 0 if it is unoccupied). V_2 is the most prominent and fundamental intrinsic defect stable at RT, and can appear in four different charge states ($+,0,-,2-$).[12,15,18,21–25] V_2 has basically a D_{3d} point-group symmetry with the high-symmetry axis along the four equivalent $\langle 111\rangle$ directions. However, in the charge states $+$, 0, and $-$, degenerate and partially occupied orbitals appear, and Jahn-Teller distortion lowers the symmetry to C_{2h}, as experimentally observed by EPR measurements performed below 20 K.[21] Above ~ 30 K, electronic bond switching between the three equivalent directions of distortion is thermally activated, and, ultimately, the switching rate is so high that the defect does not relax in the low-symmetry configurations. V_2 becomes a six-silicon-atom center, and exhibits a motionally averaged state with the effective symmetry of D_{3d}. It has previously been pointed out that the DLTS peaks associated with the different charge-state transitions of V_2 occur at high temperatures where the reorientation time for bond switching is several orders of magnitude smaller than the time for carrier emission from the V_2 levels in the band gap:[26] $E_c-0.23$ eV: $V_2(2-/-)$; $E_c-0.43$ eV: $V_2(-/0)$; $E_v+0.23$ eV: $V_2(0/+)$; where E_v is the valence-band edge. Thus the DLTS peaks caused by V_2 are attributed to the motionally averaged state and not to the distorted one with C_{2h} symmetry. Similar arguments for motional averaging hold also for the DLTS peak ascribed to the E center, which is a defect of prime importance in moderately and highly doped n-type float zone (Fz) samples.[23,27,28] Assuming phosphorus-doped samples, VP gives rise to an acceptor level ~ 0.45 eV below E_c, and can be described as a vacancy trapped next to a substitutional phosphorus atom. In the neutral charge state, two of the three silicon atoms surrounding the vacancy pull together to form an electron pair bond, leaving an unpaired electron in the orbital of the third silicon atom, while two electrons with antiparallel spins are accommodated by the phosphorus atom. When the Fermi level is above $E_c-0.45$ eV, an extra electron is accepted, and VP becomes negatively charged, possessing no unpaired electron. In fact, VP is more effective in removing electrons from the conduction band than VO, since generation of the former center removes two electrons by converting a positively charged P donor to a negatively charged VP center while generation of VO removes only one electron by converting a neutral O_i atom to a negatively charged VO center.

In this work vacancy-associated defects in n-type silicon implanted with low doses (10^7-10^{10} cm^{-2}) of ^{11}B, ^{12}C, ^{16}O, ^{28}Si, ^{74}Ge (^{76}Ge), and ^{120}Sn ions are studied using energies between 0.4 and 8.0 MeV. No defects associated with the implanted species are found, but intrinsic and impurity-related defects like V_2 and VO are identified; their generation has been studied in detail as a function of ion mass, dose, dose rate, implantation temperature, and sample depth. Immediate recombination between V's and I's plays a dominant role, and in proximity to the surface (depth of damage peak $\leqslant 1\,\mu$m), substantially narrower depth distributions than predicted by simulations are obtained. In particular, this is most pronounced for the VO centers, and the results indicate that the surface acts as a sink for migrating defects. Keeping the dose constant, a ''reverse'' dose rate dependence is observed where $[V_2]$ and $[V\mathrm{O}]$ decrease with increasing dose rate (the brackets denote concentration values). The dose rate effect depends on the ion mass, but at low enough dose rates the generation of V_2^- in the damage peak region is closely proportional to the density of elastic energy deposition for all the different types of ions studied. How-

ever, large deviations from such a proportionality occur for V_2^{2-} and VO, which actually increase in concentration at implantation temperatures between 300 and 525 K while $[V_2^{-}]$ stays constant. This temperature dependence emphasizes the importance of defect migration and lattice restoration of disordered zones for formation of unperturbed V_2 and VO centers by single-collision cascades.

The experimental data are qualitatively compared with computer simulations of the defect reaction kinetics, and discussed within the framework of a simple model where interaction between individual collision cascades is primarily due to fast-diffusing and overlapping Si self-interstitials. The interaction is most pronounced at high dose rates giving rise to enhanced annihilation of V, V_2, and VO centers because of recombination with the overlapping I's.

II. EXPERIMENTAL PROCEDURE

Samples were cut from n-type (100)-oriented Cz or Fz silicon wafers doped with phosphorus. Five different types of Cz materials were used with resistivities of 0.4 Ω cm ($\sim 1.6\times10^{16}$ P atoms/cm^3), 0.6 Ω cm ($\sim 1.0\times10^{16}$ P/cm^3), 0.7 Ω cm ($\sim 8\times10^{15}$ P/cm^3), 2 Ω cm ($\sim 2.5\times10^{15}$ P/cm^3), and 6 Ω cm ($\sim 8\times10^{14}$ P/cm^3), respectively. The resistivities of the Fz wafers were 25 Ω cm ($\sim 2\times10^{14}$ P/cm^3) and 65 Ω cm ($\sim 8\times10^{13}$ P/cm^3), respectively. According to IR-absorption measurements, performed at RT, the concentration of interstitial oxygen atoms $[O_i]$ varied between $\sim 1.7\times10^{18}$ and $\sim 7\times10^{17}$ cm^{-3} in the Cz samples while the concentration of substitutional carbon $[C_s]$ was below 2×10^{16} cm^{-3}. In the Fz samples both $[O_i]$ and $[C_s]$ were below 5×10^{15} cm^{-3}.

The samples were implanted with ^{11}B, ^{12}C, ^{16}O, ^{28}Si, ^{74}Ge (^{76}Ge), and ^{120}Sn ions at temperatures from $\sim$90 to $\sim$525 K using the 1.7 MV NEC Tandem implanter at the Australian National University. The ion energies were between 0.4 and 8.0 MeV, and the incident ion beam, having a spot diameter of $\sim$1 mm, was scanned over an aperture (2.5×4 cm^2) to ensure uniformity (horizontal scan rate 517 Hz, vertical scan rate 64 Hz). The ion doses were in the range of 5×10^7 to 2×10^{10} cm^{-2}, and the average dose rate was varied from $\sim 3\times10^7$ to 3×10^9 cm^{-2} s^{-1} by changing the scanned area while keeping the beam current constant. Careful attention was given to accurate dosimetry at the low doses used, and the error in nominal dose never exceeded 10% except under the highest dose rate conditions, where it was below 20%.

After implantation, the samples were chemically cleaned using a standard procedure which included a final dip in diluted hydrofluoric acid.[29] Immediately after cleaning, the samples were loaded into a vacuum chamber, where Schottky barrier contacts were grown at RT ($\leqslant 40$ °C) by thermal evaporation of gold through a metal mask at a base pressure less than 2×10^{-6} Torr.

The DLTS setup used is a refined version of the one described in detail in Ref. 30. The sample temperature was scanned between 77 and 300 K with a resolution of 1 K, i.e., the capacitance transients assigned to a given temperature were recorded and averaged within an interval of 1 K. The DLTS signal was extracted from the transients applying a lock-in type of weighting function, and eight traditional

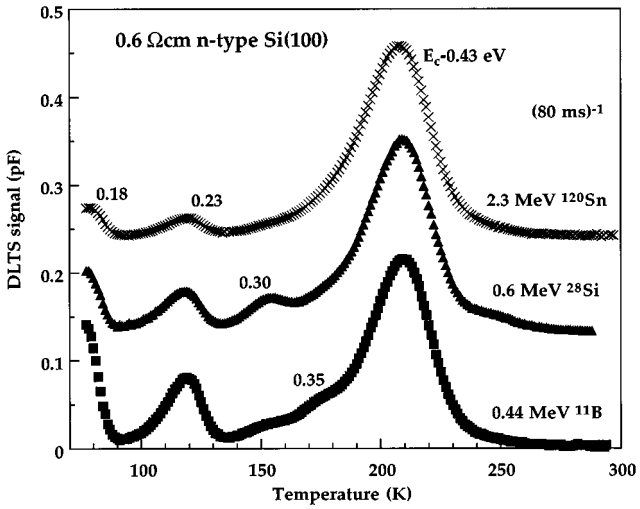

FIG. 1. DLTS spectra from three Cz samples implanted with ^{11}B, ^{28}Si, and ^{120}Sn ions, respectively. The two latter spectra are displaced for clarity. The rate window is (80 ms)$^{-1}$, and the width of the injection pulse is 10 ms.

DLTS spectra with rate windows from (20 ms)$^{-1}$ to (2.56 s)$^{-1}$ were simultaneously obtained from one single temperature scan. Concentration, energy position in the band gap, and electron-capture cross section of the observed levels were subsequently evaluated from the spectra stored in the computer memory. During all the measurements, reverse-bias conditions applied and no forward-bias injection was performed.

Concentration versus depth profiles were determined by selecting one of the eight rate windows and holding the temperature constant within ±0.5 K at the maximum of the DLTS peak of interest. The steady-state reverse bias voltage was kept constant while gradually increasing the amplitude of the majority-carrier pulse. The depth profiles were then extracted from the dependence of the DLTS signal on the pulse amplitude,[17,24] where the voltages used were converted into depth by the conventional square-root dependence for a Schottky barrier junction.[30]

III. RESULTS

Figure 1 shows DLTS spectra from three Cz samples (0.6 Ω cm) implanted at RT with 0.44-MeV ^{11}B, 0.6-MeV ^{28}Si, and 2.3-MeV ^{120}Sn ions, respectively. The dominating level is located 0.43 eV below E_c, and originates primarily from V_2^{-} with some contribution from the overlapping signal of VP. The VP center is less thermally stable than V_2,[23,28] and annealing experiments yield a relative contribution of VP to $[E_c-0.43\ \text{eV}]$ of 10–15 % in these samples. The relative strength of the level assigned to V_2^{2-} at $E_c-0.23$ eV decreases with increasing ion mass and the ratio $[E_c-0.43\ \text{eV}]/[E_c-0.23\ \text{eV}]$ deviates strongly from unity, consistent with previous findings for heavy ions.[26] Also, the peak associated with VO at $E_c-0.18$ eV decreases in relative strength with increasing ion mass, where $[E_c-0.18\ \text{eV}]$ is almost comparable to $[E_c-0.43\ \text{eV}]$ for ^{11}B ions but only $\sim$15% of $[E_c-0.43\ \text{eV}]$ for ^{120}Sn ions. Two weak peaks occur at $E_c-0.30$ and $E_c-0.35$ eV, respec-

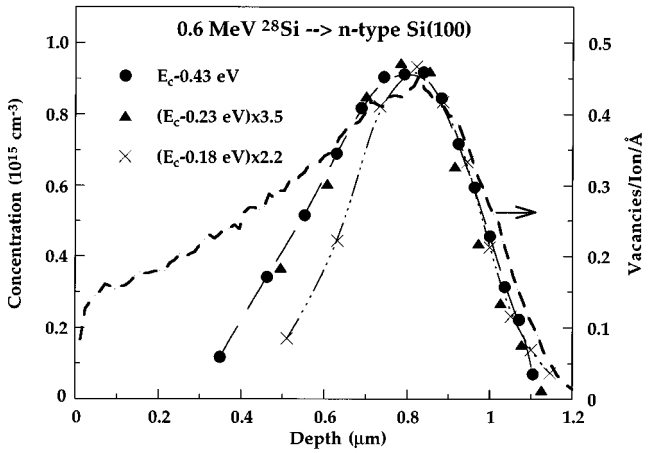

FIG. 2. Concentration vs depth profiles for the levels at 0.43, 0.23, and 0.18 eV below E_c in a sample implanted at 295 K with 1.8×10^9 Si ions/cm^2 using a dose rate of $\sim1.2\times10^8$ ions/cm^2 s. Comparison is made with the vacancy profile estimated by TRIM.

tively; the latter was discussed in detail by Jagadish, Svensson, and Hauser[31] and is due to an impurity-related center, possibly containing carbon and/or copper.[32] The origin of the $E_c-0.30$-eV level is not known but it saturates in strength at low implantation doses which strongly suggests a complex involving impurities of low concentration ($<10^{14}$ cm^{-3}) in the as-grown material.

In Fig. 2, concentration versus depth profiles are displayed for the levels at 0.43, 0.23, and 0.18 eV below E_c in a sample implanted with 0.6-MeV ^{28}Si ions to a dose of 1.8×10^9 cm^{-2}. Comparison is made with the vacancy distribution estimated from TRIM simulations, where the collision sequences induced by recoiling silicon atoms were followed to completion. In all the TRIM simulations, version 90.05 of the code was employed, and a displacement energy threshold of 13 eV was used. All four profiles in Fig. 2 peak at ~0.85 μm, but the experimental ones are more confined to the peak region with a considerably smaller tail toward the surface than predicted by TRIM. In particular, this holds for *V*O, while the profiles of the two levels primarily associated with V_2 are identical in shape and broader toward the surface than that of the $E_c-0.18$-eV level. Further evidence of the influence of the surface on the defect generation is given in Figs. 3, showing depth profiles of $[E_c-0.18$ eV$]$ in samples implanted with 0.5- and 7.3-MeV ^{12}C ions. For the deep implantation the profile peaks at ~6.6 μm [Fig. 3(b)], and the surface plays a minor role. In contrast to that in Fig. 3(a), the measured distribution in Fig. 3(b) is broader than the TRIM profile with a ~0.7-μm larger value of the full width at half maximum, and a pronounced tail toward the surface as well as into the bulk. Moreover, in Figs. 2 and 3 the absolute concentration values are much smaller than suggested by TRIM, and the total concentration of electrically active vacancy-type defects amounts only to a few percent of the calculated vacancy concentration.

A linear increase in concentration with ion dose is obtained for the levels associated with V_2 and *V*O, irrespective of the type of bombarding ion, and Fig. 4 illustrates results for 0.6-MeV ^{28}Si ions using doses up to 3×10^9 cm^{-2}. At higher doses, charge-carrier compensation by the deep-level

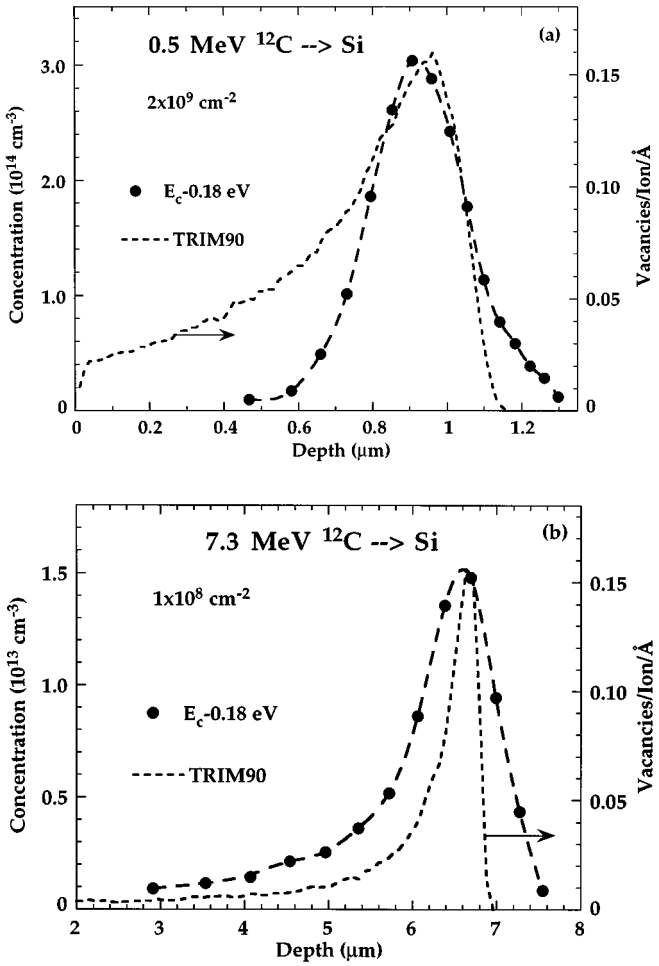

FIG. 3. Concentration vs depth profiles for the $E_c-0.18$-eV level in samples implanted with ^{12}C ions using an energy of 0.5 MeV (a) and 7.3 MeV (b). Vacancy profiles obtained by TRIM are included for comparison.

defects becomes significant, and the DLTS technique is not truly applicable. The generation of V_2 and *V*O centers depends on the dose rate, and in Fig. 5 the amplitude of the $E_c-0.43$-, $E_c-0.23$-, and $E_c-0.18$-eV levels is depicted as

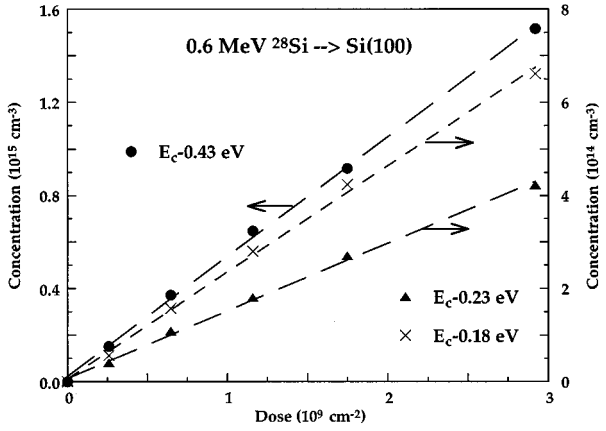

FIG. 4. Concentration of the levels at 0.43, 0.23, and 0.18 eV below E_c as a function of implantation dose at 295 K for 0.6-MeV ^{28}Si ions using a dose rate of $\sim1.2\times10^8$ ions/cm^2 s.

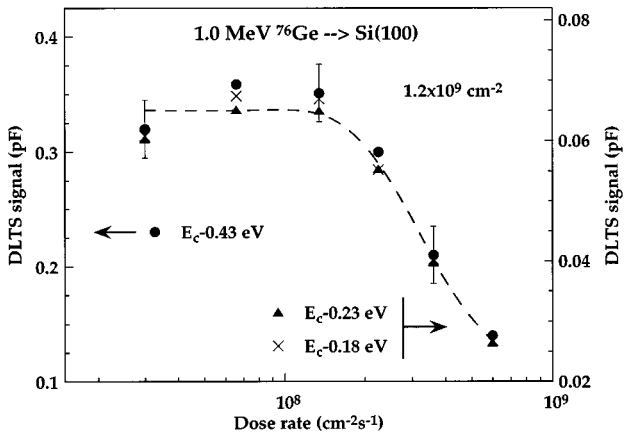

FIG. 5. Amplitudes of the levels at 0.43, 0.23, and 0.18 eV below E_c as a function of dose rate for 1.0-MeV ^{76}Ge ions, keeping the dose constant at 1.2×10^9 cm^{-2}. The implantations were performed at 295 K. At high dose rates, the error bar indicates a relative accuracy of $\pm15\%$, and is given by the accuracy of the dosimetry.

a function of dose rate for 1.0-MeV ^{76}Ge ions, keeping the dose constant at 1.2×10^9 cm^{-2}. Within the experimental accuracy, V_2 and VO exhibit an identical behavior where the amplitudes of the three levels stay constant below $\sim1\times10^8$ cm^{-2}s^{-1}, while a relative decrease by a factor of ~3 is found at $\sim6\times10^8$ cm^{-2}s^{-1}. A similar effect is also observed for the other ions, and Fig. 6 compares the results for the $E_c-0.43$-eV level after bombardment by ^{11}B, ^{28}Si, ^{76}Ge, and ^{120}Sn ions. Figure 6 reveals a mass dependence and the decrease in generation of the $E_c-0.43$-eV level shifts to higher dose rates for light ions. This trend is also consistent with data reported previously for protons,[33] showing a decrease in the defect generation at dose rates in excess of $\sim10^{10}$ cm^{-2}s^{-1}.

In Fig. 7, results are shown for the generation rate of the $E_c-0.43$- and $E_c-0.23$-eV levels in the damage peak region, and data are included for all the materials, types of ions, and ion energies employed in this study. The implantations were performed at RT, and the generation rate is extracted from the slope of the linear relation between defect concentration and ion dose obtained at low dose rates ($\leqslant10^8$ cm^{-2}s^{-1}). The generation of the $E_c-0.43$-eV level per ion-induced vacancy is identical within $\pm10\%$ for all the ions, irrespective of mass and silicon material used. The concentration of ion-induced vacancies is estimated from TRIM calculations, and assuming a displacement energy threshold of 13 eV, the absolute value of generated V_2 centers per ion-induced vacancy becomes $\sim1.1\times10^{-2}$. For the $E_c-0.23$-eV level, large deviations from a constant generation per ion-induced vacancy are observed, and a gradual decrease in the efficiency occurs for heavy ions. However, the generation of the $E_c-0.23$-eV level increases as the implantation temperature is raised above RT, while $[E_c-0.43$ eV$]$ stays constant; this is illustrated in Fig. 8 for ^{28}Si ions, where the ratio $[E_c-0.43$ eV$]/[E_c-0.23$ eV$]$ decreases from ~4.5 at temperatures below 300 K to ~2 at 500 K. Results are included for both 0.6- and 5.6-MeV ^{28}Si ions, and no energy dependence is revealed. Further, although the amplitude of the $E_c-0.43$-eV peak remains constant within $\pm10\%$ in Fig. 8, the full width at half maximum of the peak decreases from ~33 K below 300 K to ~22 K at 500 K, Fig. 9. The latter width is close to that expected theoretically (~20.6 K), and a corresponding narrowing with increasing temperature is also found for the $E_c-0.23$ eV peak (Fig. 9).

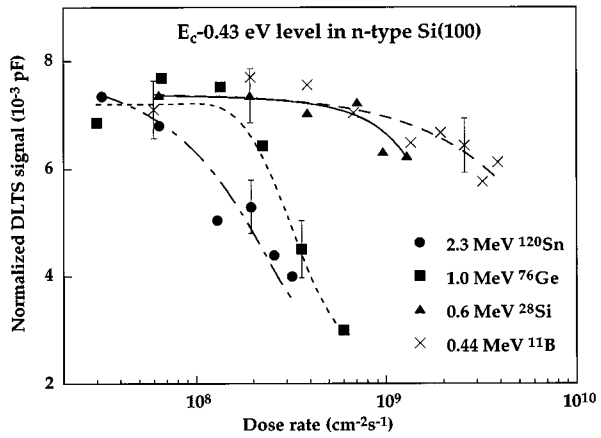

FIG. 6. The relative amplitude of the $E_c-0.43$-eV level as a function of dose rate for ^{11}B, ^{28}Si, ^{76}Ge, and ^{120}Sn ions, keeping the dose constant at 1×10^{10}, 3×10^9, 1.2×10^9, and 6×10^8 cm^{-2}, respectively. The implantations were performed at 295 K. Error bars at high dose rates indicate a relative accuracy of $\pm15\%$.

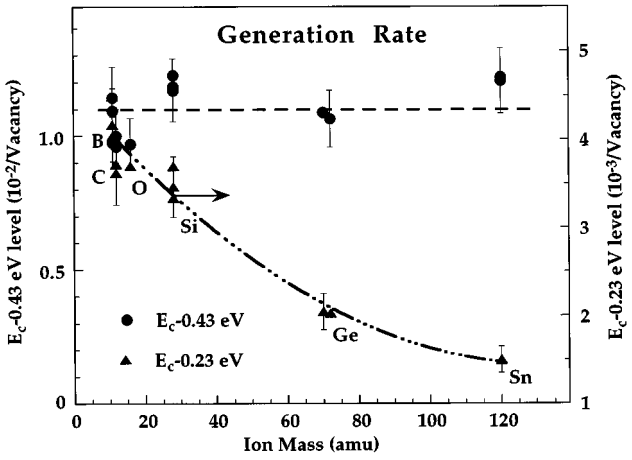

FIG. 7. Generation of the $E_c-0.43$- and $E_c-0.23$-eV levels per ion-induced vacancy in the damage peak region for bombardment at low dose rates ($\leqslant1\times10^8$ cm^{-2}s^{-1}) of Cz and Fz samples by ^{11}B, ^{12}C, ^{16}O, ^{28}Si, ^{74}Ge, ^{76}Ge, and ^{120}Sn ions. The implantations were performed at 295 K, and the concentration of ion-induced vacancies was obtained from TRIM calculations assuming a displacement energy threshold of 13 eV.

Figure 10 shows the ratio between the amplitudes of the $E_c-0.18$- and $E_c-0.43$-eV levels versus ion mass in samples implanted at RT with group-IV ions. The resistivity of the samples was 6 Ω cm, and in order to minimize surface effects and to keep the peak position of the defect distributions at a constant depth (~4.0 μm), energies between 3.6 and 8 MeV were employed for the different ions. A pronounced decrease in the generation efficiency of VO is observed with increasing ion mass, and for ^{120}Sn ions a reduc-

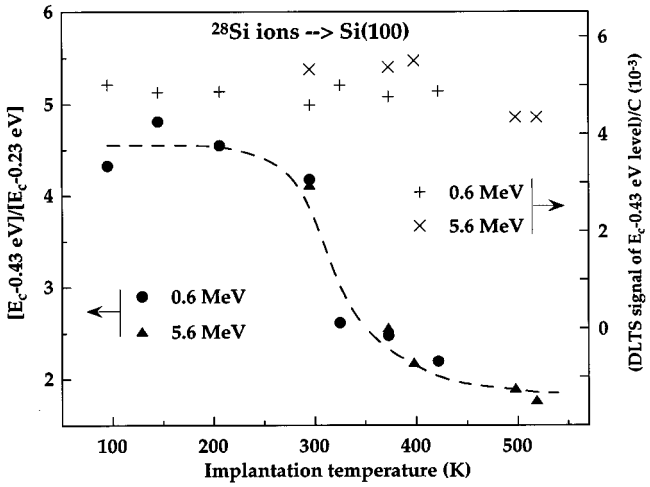

FIG. 8. Ratio between the concentrations of the $E_c-0.43$- and $E_c-0.23$-eV levels as a function of implantation temperature for 0.6- and 5.6-MeV ^{28}Si ions. The absolute amplitude of the $E_c-0.43$-eV level, normalized to the capacitance value at steady-state reverse-bias voltage during the DLTS measurements, is also shown.

tion by a factor of ~ 5 is found relative to ^{12}C ions; a similar trend is also observed in high-purity, low-doped Fz samples with the damage peak located at depths in excess of 10 μm.[34] Moreover, in analogy with the observations for the $E_c-0.23$-eV level, the generation of the $E_c-0.18$-eV level increases at elevated implantation temperatures, and for ^{28}Si ions [$E_c-0.18$ eV] is almost comparable to [$E_c-0.43$ eV] after implantation at 500 K. This is illustrated in Fig. 11, showing data from both deep (5.6 MeV) and shallow (0.6 MeV) silicon implantations; the two sets of data yield different absolute values because of surface effects, but exhibit a similar dependence on the implantation temperature.

IV. DISCUSSION AND CONCLUSIONS

No DLTS peak associated with the implanted species is found for the ions used in this study. This holds generally for all kinds of ions after low-dose bombardment of silicon at

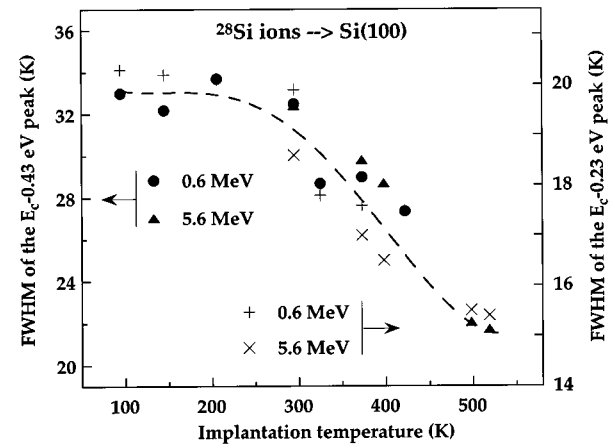

FIG. 9. Full width at half maximum (FWHM) of the $E_c-0.43$- and $E_c-0.23$-eV peaks as a function of implantation temperature for 0.6- and 5.6-MeV ^{28}Si ions.

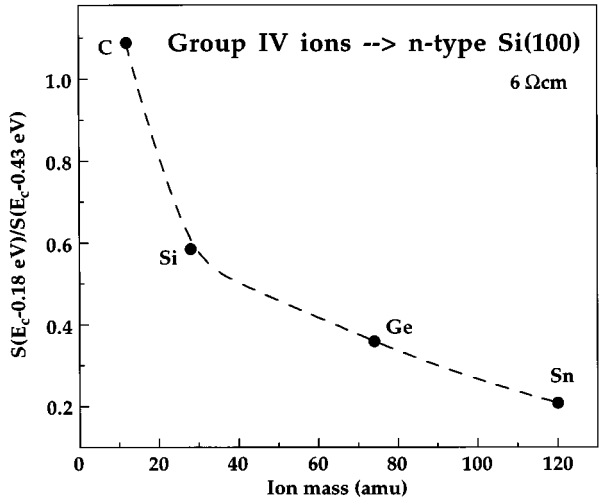

FIG. 10. Ratio between the amplitudes of the levels at $E_c-0.18$- and $E_c-0.43$-eV versus ion mass for implantation by group-IV ions at 295 K.

RT, except for protons, where two hydrogen-related levels appear at ~ 0.32 and ~ 0.45 eV below E_c.[35–37] For heavier ions than protons, the defect production per ion becomes large and the doses must be kept low in order to avoid charge-carrier compensation by deep-level defects. If the compensation exceeds $\sim 10\%$ of the free-carrier concentration, DLTS is not truly applicable, and for a dose of 10^9 cm^{-2} the peak concentration of implanted species is only of the order of 10^{13} cm^{-3}. This is very low compared to the concentration of common impurities like oxygen and carbon in as-grown silicon samples, and the probability of trapping mobile defects, as for example V's and I's, by the implanted species becomes small. Hence, unless a vast majority appears in an electrically active state directly after slowing down and coming to rest, no DLTS signal associated with the implanted species is anticipated above the detection limit.

A. Depth and dose dependence

The linear dependence on dose observed for V_2 and VO indicates a dilute concentration regime where [V_2] and

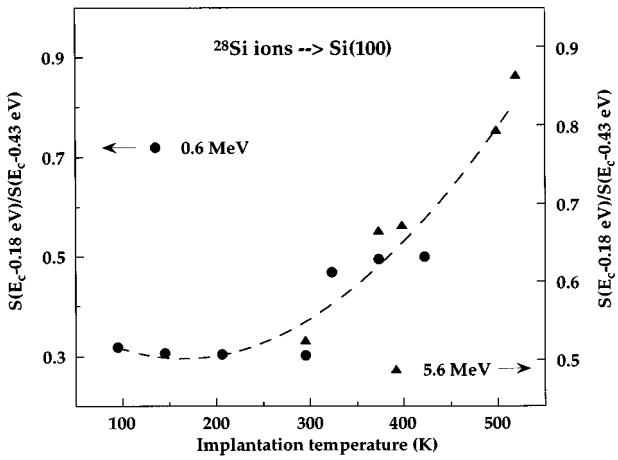

FIG. 11. Ratio between the amplitudes of the levels at $E_c-0.18$- and $E_c-0.43$-eV as a function of implantation temperature for 0.6- and 5.6-MeV ^{28}Si ions.

$[VO]$ are not high enough to influence the trapping of migrating defects, e.g., formation of high-order stable complexes through reactions with diffusing vacancies ($VO+V\rightarrow V_2O$ and $V_2+V\rightarrow V_3$), and a corresponding decrease in the effective generation rate of V_2 and VO are of minor importance. For a dose of 1×10^9 cm^{-2} the average distance between the impinging ions is $\geqslant 0.3$ μm, and the defect generation is primarily due to individual collision cascades with possible overlap of rapidly diffusing I's between adjacent cascades.[33,38]

Monovacancies are normally considered to be highly mobile in crystalline silicon at RT,[39] with a diffusion coefficient D_V of $\sim 5\times10^{-9}$ cm^2 s^{-1}. Despite the fact that vacancy diffusion is not accounted for in the TRIM calculations, the shallow depth profiles of $[V_2]$ and $[VO]$ with peak positions at $\sim 0.8-0.9$ μm [Figs. 2 and 3(a)] are considerably narrower toward the surface than the calculated vacancy profile. However, the experimental profiles with peak positions at ~ 6 μm are broader than predicted by TRIM [Fig. 3(b)], and strong evidence is obtained for surface-enhanced annihilation of the V_2 and VO centers. In particular, the effect is most pronounced for VO, where the generation process involves migration of monovacancies. For the ions used in this study (atomic mass $\geqslant 11$), the density of elastic energy deposition is relatively high, and a substantial fraction of the V_2 centers are expected to form directly in the collision cascade without requiring diffusion and pairing of monovacancies. The surface-enhanced annihilation is, therefore, less pronounced for V_2, and it is important to point out that both V_2 and VO are immobile at RT.[11,14,21]

A similar near-surface effect for the depth profiles of $[V_2]$ and $[VO]$ has been observed in MeV electron-irradiated samples where a decrease occurs gradually from a depth of ~ 2.5 μm toward the surface despite that the initial distribution of $[V]$ and $[I]$ is essentially uniform throughout the samples.[24,40] Wang, Lee, and Corbett[40] assumed that the surface acts as a perfect sink for migrating vacancies, and a relation of the form

$$[V(z)]\sim(1-\exp(-z/L_v)) \tag{1}$$

was derived for the steady-state vacancy distribution in the near-surface region applying the ordinary law of diffusion. L_v is the vacancy diffusion length, and z is the sample depth. Equation (1) is qualitatively supported by experimental data, but in order to obtain a quantitative agreement D_V must be assumed to increase with decreasing depth. A corresponding effect is also revealed for the shallow profiles of $[V_2]$ and $[VO]$ in the present study. Using the reactions described in Sec. IV B [Eq. (2)] with the surface as a perfect sink for migrating V's, induced by 0.5-MeV ^{12}C ions, and putting D_V constant as a function of depth, the surface effect on the resulting $[VO]$ profile extends only to $z\leqslant 0.2$ μm, while experimentally a substantial depletion occurs for $z\leqslant 0.7$ μm [Fig. 3(a)]. Wang, Lee, and Corbett[40] partly attributed the increase in D_V near the surface to a conversion of V from a negative to a positive charge state. However, there is no conclusive evidence for this assumption, and further studies are being pursued to elucidate the exact role of the surface during formation of vacancy-type defects.[41]

B. Dose rate effect

The decrease in generation of V_2 and VO centers with increasing dose rate (Figs. 5 and 6) is in direct contrast to that generally observed for damage buildup at doses in excess of 10^{12} cm^{-2}, and dose rates in the range $\sim 10^{11}-10^{15}$ cm^{-2} s^{-1}.[8,9,42–44] This also holds for the decrease in generation of V_2 centers with decreasing implantation temperature reported previously for ^{120}Sn ions.[38] In order to understand the reverse dose rate effect and its dependence on ion mass qualitatively, we adopted and further developed a model originally proposed by Hallén *et al.*[33] for proton bombardment. V's and I's are assumed to originate from a well-defined source from which they can spread radially. Only one dimension is considered in the calculations, and the initial sources of V's and I's are randomly distributed along an x axis perpendicular to the incident beam direction with a density corresponding to the implantation dose and a separation in arrival time by Δt. V's and I's diffuse along the x axis, and the following defect reactions are included:

$$\begin{aligned} V+I&\rightarrow\varnothing \quad \text{(annihilation)},\\ V+V&\rightarrow V_2,\\ V_2+I&\rightarrow V,\\ V+O_i&\rightarrow VO,\\ VO+I&\rightarrow O_i. \end{aligned} \tag{2}$$

This set of equations is not complete, and is only intended for a qualitative comparison with the experimental data. Several reactions which affect the absolute generation rate of V_2 and VO are omitted, and must be considered for an absolute treatment, e.g., formation of carbon-oxygen centers, carbon-carbon pairs, and direct generation of V_2 centers. In particular, for heavy ions a substantial fraction of the V_2 centers are anticipated to form directly in the dense collision cascades. The coupled differential rate equations derived from Eq. (2) are given in Table I together with the input values used in the calculations. The differential equations are numerically solved simultaneously from time $t=0$, when the first cascade is initiated, until the defects from the last ion have completed their reactions. The evolution in concentration of each defect center can be followed as a function of time and position along the x axis, and Fig. 12 shows the integrated concentration of VO centers versus the arrival rate for incoming ions of H, B, Si, and Ge. Similar to the experimental results, the production of VO decreases at high enough rates, and this occurs because of rapidly diffusing I's which overlap and annihilate V's created in adjacent ion tracks. The annihilation is enhanced when the collision cascades are generated sufficiently close in time and space. At low dose rates the distribution of $[I]$ generated by one ion becomes diluted before the arrival of later ions, since the I's have enough time to diffuse out from the space of interest and/or to form stable (immobile) complexes with other defects and impurities. The overlap of I's between different collision cascades is, therefore, of minor importance at low dose rates, and no enhanced annihilation of V's occurs.

TABLE I. Survey of the simultaneous differential rate equations for the reactions in Eq. (2) and numerical values of the input parameters used in the computations. Brackets denote concentration values, and the source terms (initial values) of the vacancy and interstitial distributions, $[V(x,0)]$ and $[I(x,0)]$, are estimated from TRIM simulations.

$$\frac{\partial[V(x,t)]}{\partial t}=D_V\frac{\partial^2}{\partial x^2}[V]-4\pi R\{(D_V+D_I)[V][I]+4D_V[V]^2-D_I[V_2][I]+D_V[V][\mathrm{O}_i]\}$$

$$\frac{\partial[I(x,t)]}{\partial t}=D_I\frac{\partial^2}{\partial x^2}[I]-4\pi R\{(D_V+D_I)[V][I]+D_I[V_2][I]+D_V[VO][I]\}$$

$$\frac{\partial[V_2(x,t)]}{\partial t}=4\pi R\{2D_V[V]^2-D_I[V_2][I]\}$$

$$\frac{\partial[VO(x,t)]}{\partial t}=4\pi R\{D_V[V][\mathrm{O}_i]-D_I[VO][I]\}$$

$$\frac{\partial[\mathrm{O}_i(x,t)]}{\partial t}=-4\pi R\{D_V[V][\mathrm{O}_i]-D_I[VO][I]\}$$

Capture radius	$R=5$ Å
Diffusion coefficients (300 K) taken from Refs. 39 and 45	$D_V=4.2\times10^{-9}$ cm^2/s $D_I=3.2\times10^{-4}$ cm^2/s
Initial values ($t=0$)	$[V_2(x,0)]=0$ $[VO(x,0)]=0$ $[\mathrm{O}_i(x,0)]=1\times10^{16}$ cm^{-3}

Furthermore, in accordance with the experimental data, the simulations reveal a mass dependence where the decrease in defect production shifts to higher dose rates with decreasing ion mass (Fig. 12). The shift appears because of an increasing size of the collision cascade for heavy ions. In the case of MeV protons the cascades at the depth of the damage peak can be represented by a step-function-like distribution

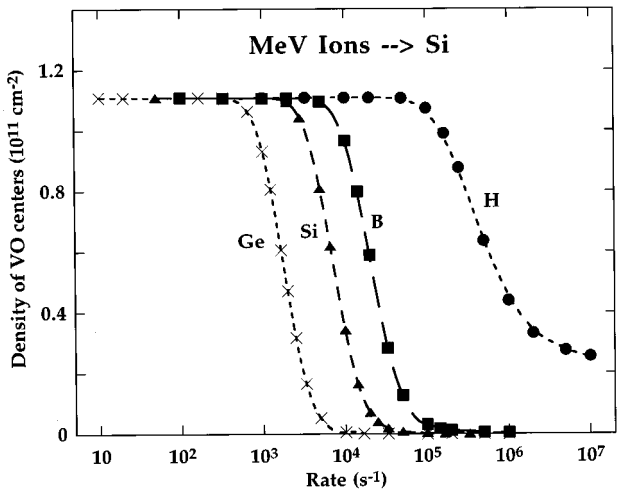

FIG. 12. Simulated values for the integrated concentration of VO centers in a layer perpendicular to the incident beam direction and at the depth of the damage peak as a function of arrival rate for MeV ions of ^{1}H, ^{11}B, ^{28}Si, and ^{74}Ge. The model used is described in the text and numerical values for the input parameters are given in Table I.

with a width of 50 Å and a density of 1×10^{18} V's and I's per cm^3, as estimated from TRIM calculations. The corresponding distribution for MeV Ge ions is of Gaussian type, with a peak concentration of 4.6×10^{18}cm^{-3} and a full width at half maximum of $\sim$6600 Å. Hence the I's induced by Ge ions have to diffuse much larger distances in order to reach a diluted concentration of I's compared to that for protons, and, since D_I is independent of the type of ion, this implies longer diffusion times in the former case. Thus overlap between adjacent collision cascades due to diffusing I's takes place during longer times for heavy ion bombardment, and the separation in arrival time between different impinging ions (Δt) at which enhanced annihilation of V's can appear becomes longer with increasing ion mass. As a result, the decrease in generation of vacancy-type defects occurs at lower rates of ion arrival ($1/\Delta t$) for heavy ions.

C. Mass and temperature dependence

For bombardment at RT by heavy projectiles like ^{74}Ge and ^{120}Sn, both experiments[46] and MD simulations[6] predict formation of amorphouslike zones by individual collision cascades, while light ions mainly produce point defects and small disordered zones. However, the results in Fig. 7 reveal a constant generation of the $E_c-0.43$-eV level per ion-induced vacancy in the damage peak region despite a relative variation in the elastic energy deposition by a factor of $\sim$16 between ^{11}B and ^{120}Sn ions. The spontaneous (correlated) recombination of V and I plays a dominant role, as shown by an absolute value of only $\sim1.1\times10^{-2}$ of generated V_2 centers per ion-induced vacancy. The spatial distribution of the V_2 centers within the individual collision cascades is not known, but our data indicate a substantial stability of the atomic configuration of V_2 even in highly damaged regions. On the other hand, the large decrease in generation of the $E_c-0.23$-eV level with increasing ion mass provides strong evidence for distorted V_2 centers. In electron-irradiated samples, where isolated point defects prevail, $[E_c-0.43\text{ eV}]$ and $[E_c-0.23\text{ eV}]$ exhibit a close one-to-one proportionality, as expected for unperturbed V_2 centers.[22,24,26] The $E_c-0.43$- and $E_c-0.23$-eV levels are attributed to a motionally averaged state of V_2 with an effective point-group symmetry of D_{3d}, but lattice strain in the damage peak region of implanted samples prevents, to a large extent, the motional averaging (electronic bond switching) of V_2. The importance of the latter effect increases for heavy ions because of a higher density of elastic energy deposition and larger distortion and strain of the crystalline silicon lattice. The electronic bond switching is a thermally activated process, and the $E_c-0.23$-eV peak, appearing at low temperatures, is, therefore, more influenced by the lattice strain than the $E_c-0.43$-eV peak. Moreover, the state of the second acceptor electron is less localized than that of the first electron because of the lower binding energy, and is anticipated to be more affected by the distorted positions of the atoms in the strained lattice.

However, the $E_c-0.43$-eV peak is also influenced by the lattice strain, as indicated by the broadening of the peak relative to that expected theoretically. The increase in peak width occurs concurrently with the relative decrease in the amplitude of the $E_c-0.23$-eV peak, and is interpreted as a

broadening of the well-defined level position associated with unperturbed V_2 centers.[26] At elevated implantation temperatures the lattice strain is gradually relaxed, and the V_2 centers become less perturbed, as shown by a substantial decrease of the ratio $[E_c-0.43\ \text{eV}]/[E_c-0.23\ \text{eV}]$ at implantation temperatures above $\sim$300 K (Fig. 8) and a narrowing of the peak widths approaching the theoretical values (Fig. 9). Here it should be emphasized that $[E_c-0.43\ \text{eV}]$ stays essentially constant for implantation temperatures between 100 and 500 K, and the decrease of the ratio $[E_c-0.43\ \text{eV}]/[E_c-0.23\ \text{eV}]$ is due to an increase of $[E_c-0.23\ \text{eV}]$, reflecting the crystalline properties of the silicon lattice surrounding the V_2 centers. These conclusions are also supported by results from MD simulations, suggesting that the disordered zones are quite unstable and tend to recrystallize easily.[6]

Similar to the $E_c-0.23$-eV level, the generation of the $E_c-0.18$-eV level per ion-induced vacancy also decreases with increasing ion mass (Fig. 10). However, the latter level does not originate from a motionally averaged state, and the decrease is mainly attributed to a true reduction in the concentration of *V*O centers. Because of the low doses used, and since O_i is a dominating impurity with $[O_i]\gg[VO]$, the generation of *V*O centers is primarily controlled by the amount of monovacancies escaping immediate recombination within the collision cascades. In fact, *V*O can be considered as a monitor for the creation of free vacancies, and is essentially a primary defect, even more elementary than V_2; indeed, this is confirmed by results from samples irradiated with MeV electrons, where the generation of *V*O centers is typically one order of magnitude higher than that of V_2.[21,24,47] Thus for a given density of energy deposited in elastic collisions, heavy ions produce less vacancies free to migrate, and fewer *V*O centers are formed than for light ions. This reveals a distinct difference between the V_2 and *V*O centers where the results for the most elementary one (*V*O) are fully consistent with predictions from MD simulations.[6] Furthermore, the increase in generation of *V*O centers at elevated implantation temperatures can be associated with the following.

(i) Relaxation of the lattice strain. The migration of *V* is promoted to form *V*O centers in a relaxed crystalline silicon lattice, and correlated recombination between *V* and *I* is less important.

(ii) Rapid recrystallization of disordered zones. These zones may have density fluctuations which upon annealing give rise to migrating point defects like *V*'s and *I*'s in the recrystallized material.[6]

Finally, it should be pointed out that the acceptor level caused by *V*O is relatively shallow, and the captured electron is not highly localized. This implies a rather perfect crystalline lattice surrounding the *V*O center for a well-defined $E_c-0.18$-eV level to appear, and may partly explain the relative decrease in generation of the level for heavy ions.

V. SUMMARY

The generation of V_2 and *V*O centers in monocrystalline silicon samples bombarded with MeV ions has been studied in detail. Because of the low doses used, the defects are primarily created by single-collision cascades and a strong surface-enhanced annihilation of the V_2 and *V*O centers are observed. In particular, the surface effect is most pronounced for *V*O, where the formation process involves migration of monovacancies. If the surface is assumed to act as a perfect sink for diffusing monovacancies, simulations of the defect reaction kinetics show that the diffusion coefficient D_V must increase toward the surface in order to obtain a quantitative agreement with the experimental data.

A linear dependence on dose is observed, but at high enough dose rates the generation efficiency of V_2 and *V*O centers per incoming ion decreases. The dose rate at which the decrease occurs shifts to lower values with increasing ion mass. This mass dependence is attributed to the increasing size of the collision cascades for heavy ions, as supported by computer simulations of the defect reaction kinetics using a model where the interaction and/or overlap between individual collision cascades is primarily due to fast-diffusing *I*'s. Because of the large collision cascades induced by heavy ions, it takes long times to dilute the concentration of overlapping *I*'s, and hence, these *I*'s can enhance the annihilation of *V*'s in adjacent cascades even for low rates of ion arrival compared to that for light ion bombardment.

The formation of V_2 and *V*O centers display a distinctly different dependence on ion mass; at low dose rates ($\leqslant 10^8\ \text{cm}^{-2}\,\text{s}^{-1}$) the generation of the former one per ion-induced vacancy stays constant for all the types of ions used in this work, whereas that of *V*O decreases with increasing ion mass. The results for *V*O are consistent with the picture that light ions are more effective in generating point defects while the data for V_2 suggest that the atomic configuration of V_2 is stable even in highly disordered regions. The V_2 centers are, however, strongly perturbed, as demonstrated by large deviations from unity of the ratio $[E_c-0.43\ \text{eV}]/[E_c-0.23\ \text{eV}]$ and broadening of the DLTS peaks. After implantation at elevated temperatures the V_2 centers are less perturbed, and appear in a silicon lattice where the bombardment-induced strain is gradually relaxed. Concurrently, more monovacancies free to migrate and form stable *V*O centers are generated, as shown by a substantial increase in $[VO]$ for implantation temperatures above 300 K.

ACKNOWLEDGMENTS

Numerous and enlightening discussions during several years with the late Professor James W. Corbett are gratefully acknowledged. The authors are also indebted to Professor James S. Williams and Niclas Keskitalo for clarifying discussions and fruitful collaboration. Financial support was received from the Swedish Natural Science Research Council, the Swedish Board for Technical Development (NUTEK), and the Australian Department of Industry, Science and Technology.

*Present address: Royal Institute of Technology, Solid State Electronics, P.O. Box E229, S-16440 Kista-Stockholm, Sweden.
[1] J. Lindhard, V. Nielsen, M. Scharff, and P. V. Thomsen, K. Dan. Vidensk. Selsk. Mat. Fys. Medd. **33**, 14 (1963).
[2] J. J. Loferski and P. Rappaport, Phys. Rev. **111**, 432 (1958).
[3] J. P. Biersack and L. G. Haggmark, Nucl. Instrum. Methods **174**, 257 (1980); J. F. Ziegler, J. P. Biersack, and U. Littmark, in *The Stopping and Range of Ions in Solids*, edited by J. F. Ziegler (Pergamon, New York, 1985), Vol. 1.
[4] See, e.g., J. M. Poate and J. S. Williams, in *Ion Implantation and Beam Processing*, edited by J. S. Williams and J. M. Poate (Academic, Sydney, 1984), p. 13.
[5] B. G. Svensson, C. Jagadish, and J. S. Williams, Nucl. Instrum. Methods Phys. Res. Sect. B **80/81**, 583 (1993).
[6] M. J. Caturla, T. Diaz de la Rubia, and G. H. Gilmer, Nucl. Instrum. Methods Phys. Res. Sec. B **106**, 1 (1995).
[7] M. L. Swanson, J. R. Parsons, and C. W. Hoelke, Radiat. Eff. **9**, 249 (1971).
[8] F. W. Morehead and B. L. Crowder, Radiat. Eff. **6**, 27 (1970).
[9] See, e.g., F. Priolo and E. Rimini, Mater. Sci. Rep. **5**, 319 (1990), and references therein.
[10] K. Kyllesbech Larsen, V. Privitera, S. Coffa, F. Priolo, S. U. Compisano, and A. Carnera, Phys. Rev. Lett. **76**, 1493 (1996).
[11] J. W. Corbett, G. D. Watkins, R. M. Chrenko, and R. S. McDonald, Phys. Rev. **121**, 1015 (1961).
[12] L. J. Cheng, J. C. Corelli, J. W. Corbett, and G. D. Watkins, Phys. Rev. **152**, 761 (1966).
[13] A. H. Kalma and J. C. Corelli, Phys. Rev. **173**, 734 (1968).
[14] G. D. Watkins and J. W. Corbett, Phys. Rev. **121**, 1001 (1961).
[15] J. W. Corbett and G. D. Watkins, Phys. Rev. Lett. **7**, 314 (1961).
[16] G. Davies and R. C. Newman, in *Handbook of Semiconductors*, edited by T. S. Moss and S. Mahajan (Elsevier, Amsterdam, 1994), p. 1557, and references therein.
[17] D. V. Lang, J. Appl. Phys. **45**, 3023 (1974).
[18] J. G. deWit, E. G. Sieverts, and C. A. J. Ammerlaan, Phys. Rev. B **14**, 3494 (1976).
[19] G. Bemski, J. Appl. Phys. **30**, 1195 (1959).
[20] G. D. Watkins, J. W. Corbett, and R. M. Walker, J. Appl. Phys. **30**, 1198 (1959).
[21] G. D. Watkins and J. W. Corbett, Phys. Rev. **138**, A543 (1965).
[22] A. O. Evwaraye and E. Sun, J. Appl. Phys. **47**, 3776 (1976).
[23] L. C. Kimerling, in *Radiation Effects in Semiconductors 1976*, edited by N. B. Urli and J. W. Corbett, IOP Conf. Proc. No. 31 (Institute of Physics and Physical Society, Bristol, 1977), p. 221.
[24] B. G. Svensson and M. Willander, J. Appl. Phys. **62**, 2758 (1987).
[25] J. H. Svensson, B. G. Svensson, and B. Monemar, Phys. Rev. B **38**, 4192 (1988).
[26] B. G. Svensson, B. Mohadjeri, A. Hallén, J. H. Svensson, and J. W. Corbett, Phys. Rev. B **43**, 2292 (1991).
[27] G. D. Watkins and J. W. Corbett, Phys. Rev. **134**, A1359 (1964).
[28] S. D. Brotherton and P. Bradley, J. Appl. Phys. **53**, 5720 (1982).
[29] M. A. Taubenblatt, D. Thomson, and C. R. Helms, Appl. Phys. Lett. **44**, 895 (1984).
[30] B. G. Svensson, K.-H. Rydén, and B. M. S. Lewerentz, J. Appl. Phys. **66**, 1699 (1989).
[31] C. Jagadish, B. G. Svensson, and N. Hauser, Semicond. Sci. Technol. **8**, 481 (1993).
[32] J. Lalita, C. Jagadish, M. O. Aboelfotoh, and B. G. Svensson (unpublished).
[33] A. Hallén, D. Fenyö, B. U. R. Sundqvist, R. E. Johnson, and B. G. Svensson, J. Appl. Phys. **70**, 3025 (1991).
[34] A. Hallén and B. G. Svensson, Nucl. Instrum. Methods Phys. Res. Sect. B **80/81**, 106 (1993).
[35] K. Irmscher, H. Klose, and K. Maass, J. Phys. C **17**, 6317 (1984).
[36] M. Hüppi, J. Appl. Phys. **68**, 2702 (1990).
[37] B. G. Svensson, A. Hallén, and B. U. R. Sundqvist, J. Mater. Sci. Eng. B **4**, 285 (1989).
[38] B. G. Svensson, C. Jagadish, and J. S. Williams, Phys. Rev. Lett. **71**, 1860 (1993).
[39] G. D. Watkins, in *Radiation Effects in Semiconductors*, edited by F. L. Vook (Plenum, New York, 1968), p. 67; J. A. van Vechten, Phys. Rev. B **10**, 1482 (1974).
[40] K. L. Wang, Y. H. Lee, and J. W. Corbett, Appl. Phys. Lett. **33**, 547 (1978).
[41] B. G. Svensson, N. Keskitalo, A. Hallén, and J. Lalita (unpublished).
[42] F. Eisen and B. Welch, Radiat. Eff. **7**, 143 (1971).
[43] G. Holmén, A. Burén, and P. Högberg, Radiat. Eff. **24**, 51 (1975).
[44] T. E. Haynes and O. W. Holland, Appl. Phys. Lett. **59**, 452 (1991).
[45] S. Mottet and Roizes, in *Defects and Radiation Effects in Semiconductors*, edited by J. H. Albany, IOP Conf. Proc. No. 46 (Institute of Physics and Physical Society, Bristol, 1978), p. 281; G. S. Oehrlein, I. Krafczik, J. L. Lindström, A. E. Jaworowski, and J. W. Corbett, J. Appl. Phys. **54**, 179 (1983).
[46] L. M. Howe and M. H. Rainville, Nucl. Instrum. Methods **182/183**, 143 (1981).
[47] J. W. Corbett and G. D. Watkins, Phys. Rev. **138**, A555 (1965).